Chemical Science

ROYAL SOCIETY OF CHEMISTRY

EDGE ARTICLE

View Article Online
View Journal | View Issue

Cite this: *Chem. Sci.*, 2024, **15**, 12819

All publication charges for this article have been paid for by the Royal Society of Chemistry

Boron-doped double [6]carbohelicenes: a combination of helicene and boron-doped π-systems†

Yujia Liu, Liuzhong Yuan, Zengming Fan, Jingyuan Yang, Yue Wang and Chuandong Dou *

Helicenes, featuring unique helical structures, have a long history as three-dimensional polycyclic aromatic hydrocarbons (PAHs). Incorporation of heteroatoms into helicenes may alter their electronic structures and achieve unexpected physical properties. Here, we disclose fusion of boron-doped π-systems onto helicenes as an efficient strategy to design boron-doped carbohelicenes. Two boron-doped double [6] carbohelicenes were synthesized, which possess the $C_{58}B_2$ and $C_{86}B_2$ polycyclic π-skeletons containing two [6]helicene subunits, respectively. The $C_{86}B_2$ molecule thus represents the largest-size helicene-based boron-doped PAH. A thorough investigation reveals that the helicene moieties and boron atoms endow the polycyclic π-systems with delocalized electronic structures, and well-tunable ground-state and excited-state photophysical properties. It is notable that the $C_{58}B_2$ molecule displays excited-state stimulated emission behavior and amplified spontaneous emission (ASE) properties in not only the blend films with various doped concentrations but also the pure film. To our knowledge, it is the first example of ASE-active [*n*]helicene ($n \geq 6$), and moreover, such robust ASE performance has rarely been observed in PAHs, demonstrating the promising utility of boron-doped carbohelicenes for laser materials.

Received 13th May 2024
Accepted 7th July 2024

DOI: 10.1039/d4sc03124e

rsc.li/chemical-science

Introduction

Polycyclic aromatic hydrocarbons (PAHs) have received much attention because of their intriguing optical, electronic and magnetic properties, as well as potential applications in organic light-emitting diodes (OLEDs), organic field-effect transistors (OFETs), organic solar cells (OSCs), *etc.*[1–8] Owing to the great advance of synthetic chemistry, various π-extended PAHs with well-defined sizes, edge structures and conformations have been successfully developed, in which their electronic structures and physical properties are mainly determined by their topological conjugated structures.[9–16] In particular, by controlling the zigzag, armchair and/or cove edge states, stimulated emission (SE) behaviors and amplified spontaneous emission (ASE) properties have been remarkably achieved in PAHs, demonstrating that they will be a promising class of optical-gain materials for organic lasers, photonics and optoelectronics.[17–20] However, as large-size topologies and zigzag edge structures usually lead to open-shell electronic states and non-fluorescence nature,[21–23] such ASE-active PAHs are still rare and limited to only a few examples, such as dibenzo[hi,st]ovalene, zigzag-edged nanographenes and molecular ribbons.[24–29] Therefore, it is needed to develop new ASE-active PAH systems, and moreover, this research may further promote the development of PAH chemistry and materials.

Helicenes, helically *ortho*-fused polyaromatics, have a long history as three-dimensional PAHs.[30] Their helical structures can induce unique intrinsic chirality despite the absence of asymmetric carbons and chiral centers, and thereby bestow interesting nonplanarity, optical rotation and dynamic behaviors, as well as other physical-organic properties.[31,32] Until now, π-extension of simple helicenes, *e.g.* [5]helicene and [6]helicene, has led to a variety of helicene systems with amazing topological structures, including elongated helicenes, multiple helicenes and expanded helicenes, such as **A**,[33] **B** (ref. 34) and **C** (ref. 29) (Fig. 1a).[33–41] Moreover, their outstanding optical, electrical and chiroptical properties, as well as synthetic chemistry and material applications have been intensively studied. Nevertheless, aside from these wonderful helicene research studies, the new space of helicene systems still needs to be explored.

Boron atoms have one less electron than carbon atoms, and feature a characteristic vacant p-orbital. Boron-doping of PAHs as a powerful strategy has generated a large family of boron-doped PAHs, which not only displayed some unusual properties, such as Lewis acidity, control over supramolecular polymerization, photo-responsive fluorescence and dynamic modulation of (anti)aromaticity and diradical properties, but

State Key Laboratory of Supramolecular Structure and Materials, College of Chemistry, Jilin University, Changchun 130012, P. R. China. E-mail: chuandong@jlu.edu.cn

† Electronic supplementary information (ESI) available: Experimental details, synthesis and characterization of **1**, **2** and **6**. See DOI: https://doi.org/10.1039/d4sc03124e

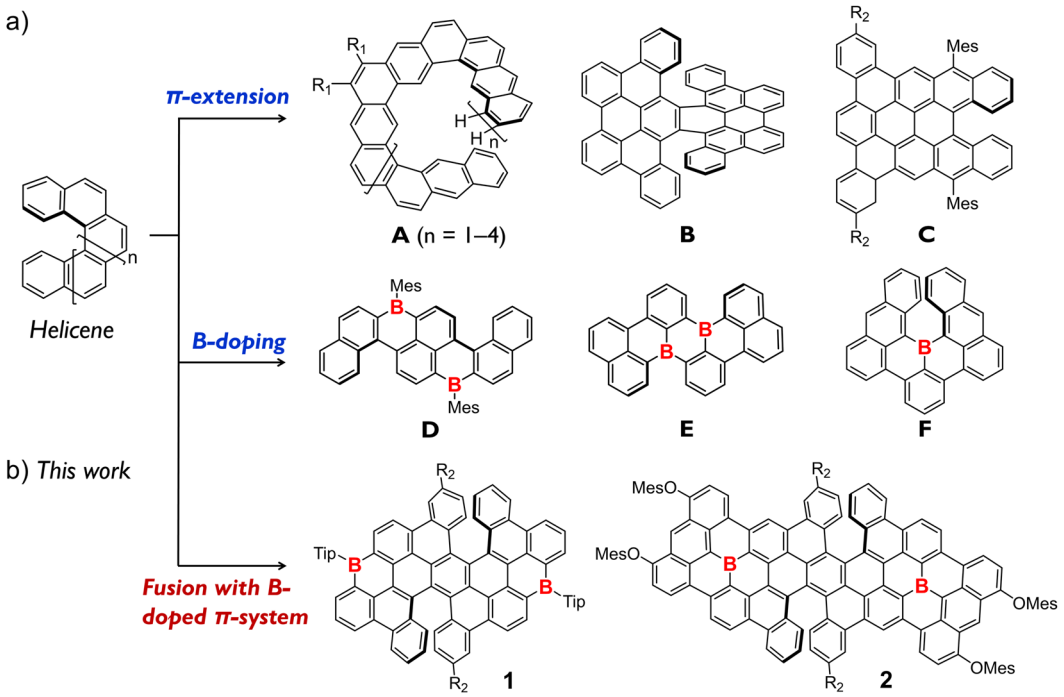

Fig. 1 (a) Schematic illustration for π-extension and boron-doping of helicenes, and representative examples of π-extended helicenes and boron-doped helicenes. (b) Design strategy for boron-doped carbohelicenes and chemical structures of **1** and **2** (this work). R_1 = O*n*Bu; R_2 = *t*Bu; Tip = 2,4,6-triisopropylphenyl; Mes = 2,4,6-trimethylphenyl.

also were employed as organic catalysts and optoelectronic materials.[42–45] However, owing to the inherent high reactivity of the boron moiety and complicated multi-step syntheses, the design and synthesis of boron-doped PAHs with large-size π-frameworks and/or well-tuned edge structures remains challenging.[46–54] For instance, only a few pristine boron-doped helicene derivatives (such as **D** and **E**) have been developed.[55–57] Moreover, most of them are based on [4]helicene, and until very recently, only one boron-doped [6]helicene **F** was constructed.[57] We recently developed several large-size boron-doped PAHs *via* implementing controllable cyclization on conjugated organoboranes.[58–60] Among them, two boron-doped [4]carbohelicenes exhibit intriguing ASE activity in the blend films.[61,62] We thus envisioned that precise control over topological structures of boron-doped PAHs may afford not only more sophisticated π-scaffolds but also organic emitters with desirable ASE performance.

Herein, we disclose fusion of boron-doped π-systems onto helicenes as an efficient strategy to design boron-doped carbohelicenes. Two boron-doped double [6]carbohelicenes **1** and **2** (Fig. 1b) that feature fully fused $C_{58}B_2$ and $C_{86}B_2$ π-conjugated frameworks containing two [6]helicene subunits, respectively, were successfully synthesized. Thus, we achieved a combination of helicene and boron-doped π-systems and created the largest-size record of helicene-based boron-doped PAHs. Their molecular geometries, aromaticity and electronic structures, as well as ground-state and excited-state photophysical properties have been studied in detail. Notably, the $C_{58}B_2$ molecule displays stimulated emission behavior and amplified spontaneous emission properties in the various blend films and even pure film, which have rarely been achieved in PAHs. Therefore, this study provides not only two new examples of boron-doped carbohelicenes, but also opens a new direction for the design of functional helicenes and efficient ASE-active PAHs using organoboron chemistry.

Results and discussion

As shown in Scheme 1, the target B-doped carbohelicenes **1** and **2** were synthesized starting from two key B-containing building blocks **3** and **4**, which were first reported by Feng's group and our group, respectively.[61,63] The Suzuki–Miyaura cross-coupling reactions between **3**/**4** and 2,5-di-(4-*tert*-butylphenyl)-1,4-bis-bpin-benzene produced the precursors **5**/**7**. The oxidative cyclization reaction of **5** with 2,3-dichloro-5,6-dicyano-1,4-benzoquinone (DDQ) and CH_3SO_3H in dry CH_2Cl_2 led to the cyclization of rings B and G, and generated a partially fused product **6**. The Scholl reaction with $FeCl_3$ was then performed on **6**, yielding compound **1** *via* the cyclization of rings A and D. Based on these synthetic results, we treated compound **7** with $FeCl_3$ and directly prepared the desired product **2** with a larger size. Compounds **1** and **2** were purified using silica gel column chromatography without any special precautions (Fig. S1†). As determined by high-resolution mass spectrometry (HRMS), only one intense peak is observable in their HRMS spectra, and the experimental isotopic distributions agree well with the stimulated data, thus confirming the molecular formula of $C_{96}H_{88}B_2$ for **1** and $C_{130}H_{92}B_2O_4$ for **2** (Fig. S2†).

The conformations of B-doped carbohelicenes **1** and **2** were studied by density functional theory (DFT) calculations at the

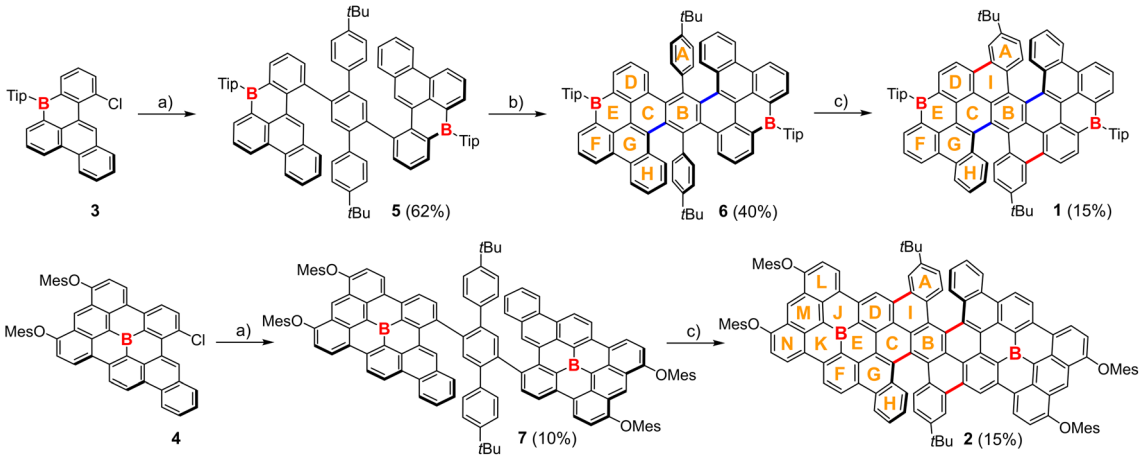

Scheme 1 Synthesis of **1** and **2**. Reagents and conditions: (a) 2,5-di-(4-*tert*-butylphenyl)-1,4-bis-bpin-benzene, $Pd(PPh_3)_4$, Sphos, K_3PO_4, toluene : C_2H_5OH : H_2O; (b) DDQ, CH_3SO_3H, CH_2Cl_2, 0 °C; (c) $FeCl_3$, CH_3NO_2, CH_2Cl_2, 25 °C.

B3LYP/6-311G(d) level of theory. For **1**, there are three possible stereoisomers, including 1-(*P*,*P*), 1-(*P*,*M*) and 1-(*M*,*M*) (Fig. 2 and S4†). The optimized geometries of 1-(*P*,*P*) and 1-(*M*,*M*) have the $C_{58}B_2$ π-frameworks, which are composed of two [6]helicene substructures and two B-containing π-systems with the B atoms doped into the zigzag edges (Fig. S5†). The dihedral angles are *ca.* 58° for the terminal rings of [6]helicene moieties, leading to their highly twisted conformations. As shown in the energy diagram, the enantiomers 1-(*P*,*P*) and 1-(*M*,*M*) are thermodynamically more stable than 1-(*P*,*M*) with the meso form by 2.2 kcal mol^{-1}. Additionally, the clean proton signals in the ^1H NMR spectrum of **1** are consistent with the theoretical data of 1-(*P*,*P*) (Fig. S3†). These results indicate that 1-(*P*,*P*) and 1-(*M*,*M*) were obtained as the sole products in the synthetic process. The interconversion from 1-(*P*,*P*) to 1-(*P*,*M*) proceeds through the transition state (1-TS1) with face-to-face oriented terminal rings of [6]helicene subunits. The activation free energy (45.7 kcal mol^{-1}) for 1-TS1 is much higher than that of [6]helicene, also higher than that of [7]helicene, and comparable with that of double [6]helicene **B**.[34] These B-doped carbohelicenes thus may preserve the rigidity of helicenes and thereby bestow high isomerization barriers. For **2**, its optimized (*P*,*P*)-geometry has the $C_{86}B_2$ π-framework, comprising two [6]helicene substructures and two larger B-centered π-systems (Fig. S5†). To our knowledge, compound **2** represents the largest-size helicene-edged B-doped PAHs.

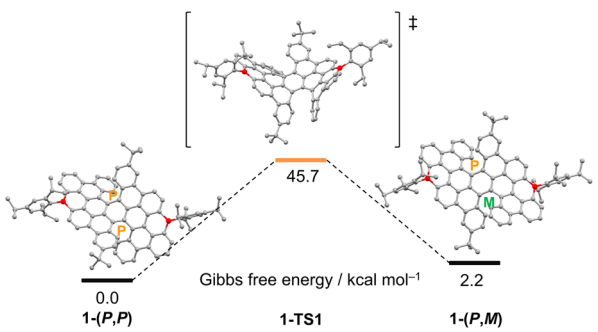

Fig. 2 Energy diagram for the isomerization from 1-(*P*,*P*) to 1-(*P*,*M*), calculated at the B3LYP/6-311G(d) level of theory.

To illustrate the electronic structures of B-doped carbohelicenes, we investigated the aromaticity of **1** and **2** along with the partially fused **6**, using nucleus independent chemical shift (NICS) and anisotropy of the induced current density (ACID) calculations at the B3LYP/6-311+G(d) and B3LYP/6-311G(d) levels, respectively.[64] The optimized (*P*,*P*)-geometries of **1** and **2** were employed as the model structures for the calculations. As shown in Fig. 3, largely negative $NICS(1)_{ZZ}$ values are observed for rings A/B/D/F/H (in red) in **6** and **1**, and rings A/B/D/F/H/M (in red) for **2**, suggestive of their essence of aromatic sextet rings. The corresponding molecular forms of **6**, **1** and **2** shown in Scheme 1 mainly contribute to their electronic structures. In the ACID plots, the π electrons of **6** display obviously localized and clockwise ring current circuits, thus indicating its typical local aromaticity. For **1**, its π electrons are mainly delocalized along the periphery with a clockwise current, and also flow along the new C–C bonds between rings A and D. It is notable that the π electrons cross over the central ring B, which acts as a special bridge that effectively connects the two B-containing π-skeletons. Thus, different from **6**, B-doped carbohelicene **1** exhibits unusual crossed-circle aromaticity and efficient π-delocalization. For **2**, clockwise ring currents along the larger-size periphery and bypassing through ring B are observed, indicating the contribution of π-extension to molecular aromaticity. It can be concluded that the central hexagon in these two B-doped helicenes is a crucial bridge, which links two B-containing moieties and contributes to the formation of two helical substructures, further producing delocalized π-electronic structures.

Reflecting efficient π-conjugated structures, B-doped carbohelicenes **1** and **2** exhibit red-shifted and broad absorption bands. In toluene, **1** shows an absorption band that covers the range of 300–630 nm and the longest absorption maximum (λ_{abs}) at 591 nm (Fig. 4a and S7,† and Table 1). For **6**, it shows an absorption band around 300–530 nm with one intense peak at

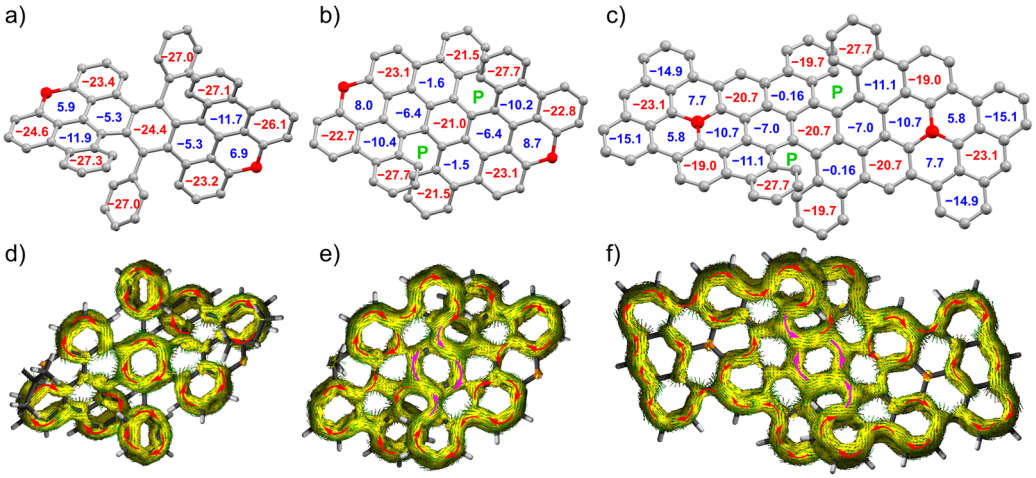

Fig. 3 Calculated NICS(1)$_{ZZ}$ values and ACID plots (contribution from π electrons only) of (a and d) **6**, (b and e) **1** and (c and f) **2**. The *t*Bu, Mes and OMes groups are removed for clarity.

453 nm and a shoulder band at 490 nm. Compared with that of **6**, the absorption spectrum of **1** is red-shifted exceeding 100 nm, despite the formation of only two more C–C bonds, thus highlighting the importance of its efficient π-conjugation. In the absorption spectrum of **2**, a broader absorption band around 300–740 nm is observed, along with a λ_{abs} of 700 nm. The unchanged time-dependent absorption spectra reveal their high ambient stability (Fig. S9†). Based on the absorption onsets, the optical band gap (E_g^{opt}) is estimated to be 2.41 eV for **6**, 1.99 eV for **1** and 1.68 eV for **2**, respectively. On the other hand, toluene solutions of **6** and **1** emit bright green and red fluorescence, respectively, with a maximum emission wavelength (λ_{em}) and fluorescence quantum yield (Φ_F) of 513/547 nm and 0.21 for **6** and 618/650 nm and 0.22 for **1**. The fluorescence bands exhibit small solvent effects on the solvent polarity (Fig. S7†). For **2**, the fluorescence is not detected in its solution. The photophysical properties of **1** are distinct from those of all-carbon double [6] helicene **B** (λ_{abs}, 506 nm; λ_{em}, 525 nm in chloroform) and B-doped double [5]carbohelicene $C_{56}B_2$ (λ_{abs}, 477 nm; λ_{em}, 504 nm in toluene),[34,61] thus demonstrating the significant effects of B-doping and π-electron delocalization.

Time-dependent density functional theory (TD-DFT) calculations were performed at the B3LYP/6-311G(d) level of theory to further reveal their absorption properties and electronic structures. The LUMOs and HOMOs of **6** and **1** are delocalized over their polycyclic frameworks, respectively (Fig. 4b). From **6** to **1**, the HOMO level is enhanced by 0.16 eV and the LUMO level is decreased by 0.41 eV, leading to the decreased energy gap, which can be ascribed to the effect of π-extension on **1**. The all-carbon analogue **1C** was employed for comparison. From **1C** to **1**, the LUMO and HOMO energies are lowered by 0.71 and 0.36 eV, respectively, and the energy gap is decreased by 0.35 eV. These changes are attributed to the B atoms in **1**, whose vacant p-orbitals obviously contribute to the LUMO and HOMO, thus implying the vital role of B-doping in the electronic structure of carbohelicene. Compared with **1**, **2** exhibits higher LUMO and HOMO energies by 0.19 and 0.55 eV, respectively, along with a narrower band gap. According to the TD-DFT calculations, the calculated transition energies, wavelengths and oscillator strengths reproduce well with the experimental spectra of **6**, **1** and **2**. It is notable that all of their low-energy absorption bands involve the HOMO → LUMO transitions, in which the B atom

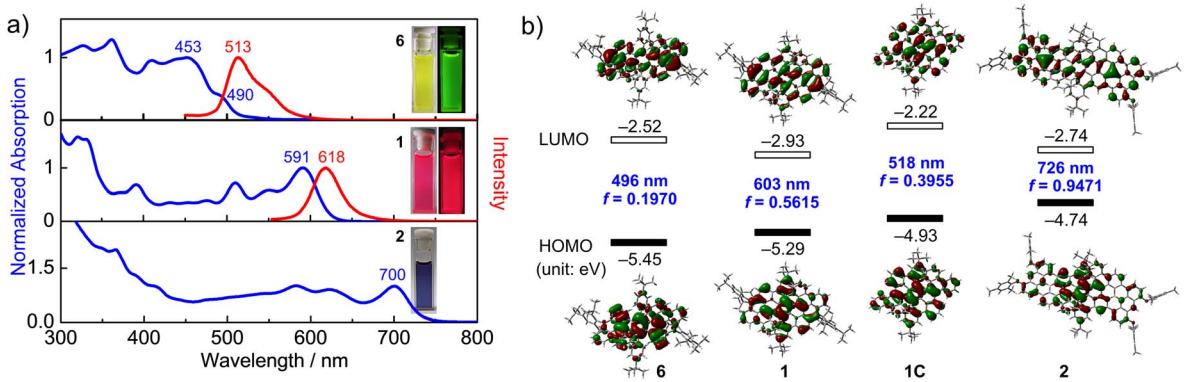

Fig. 4 (a) Absorption (blue) and fluorescence (red) spectra of **6**, **1** and **2** in toluene, along with their photographs under daylight (left) and UV-light (right). (b) TD-DFT calculations of **6**, **1**, **1C** and **2** at the B3LYP/6-311G(d) level of theory and their Kohn–Sham HOMOs and LUMOs.

Table 1 Summary of the photophysical properties of **1**, **2** and **6**

	λ_{abs}[a] [nm]	ε_{max}[a] [M^{-1} cm^{-1}]	λ_{em}[a] [nm]	λ_{SE}[b] [nm]	λ_{ASE}[b] [nm]
6	490/453	1.45×10^4	513/547	—	—
1	591/548	2.83×10^4	618/650	675	676
2	700/623	1.13×10^4	—	—	—

[a] In toluene solution (1×10^{-5} M). [b] Doped into the polystyrene film (20 wt%).

contributes to the LUMOs (Fig. S14–S16†). For **2**, its HOMO is mainly localized on the central region of the π-skeleton, whereas the LUMO is obviously distributed on the B-containing moieties. This suggests that the non-emission essence of **2** is ascribed to its intramolecular charge transfer process. Moreover, the calculated low-energy absorption of **1C** appears at 518 nm (Fig. S17†). This demonstrates that B-doping and π-extension greatly impact the red-shifted absorption properties of B-doped carbohelicenes.

To gain insight into their excited-state photophysical properties, we performed femtosecond transient absorption (fs-TA) characterization on **6**, **1** and **2**. In the wide-range fs-TA spectra, **6** and **2** in toluene exhibit ground-state bleach (GSB) signals around 459/492 nm and 640/705 nm, respectively, which agree well with their characteristic absorption signals in the steady-state absorption spectra (Fig. 5). Excited-state absorption (ESA) bands are observed at 500–750 nm for **6** and 475–615 nm for **2**. By contrast, **1** exhibits a distinctive fs-TA spectrum. Two peaks at 510/547 nm and one overwhelming band around 584–623 nm are observable, which are tentatively ascribed to the GSB regions. The ESA bands appear at 450–495 and 715–750 nm. It is notable that one unexpected negative bump at 675 nm is observed. As this signal is not present in the steady-state absorption spectrum but seems to be the long-wavelength tail of the fluorescence spectrum, we can assign it to the stimulated emission characteristic of **1**.[18,19] Thus, compound **1** features unique SE behavior in the excited state. We further conducted fs-TA measurements on the **1**/polystyrene (PS) blend film (20 wt%) and the pure film of **1**. The two films show not only GSB signals around 600 nm but also weak SE bands around 675 nm. Such preserved SE performance may be owing to less non-radiative decays in the inert PS matrix film, and weak molecular aggregation and an inhibited intermolecular charge-transfer process in the pristine film (Fig. S10,† *vide infra*).

The intriguing excited-state SE behavior of **1** promotes us to explore its amplified spontaneous emission properties, because ASE is not only a photonics process where the spontaneous emission is amplified owing to the optical-gain action but also a basic requirement for lasing materials.[65–67] The ASE characteristics of the **1**/PS blend film (20 wt%) are shown in Fig. 6a and b. Enhancing the pump laser energy over a certain threshold leads to the appearance of an emission peak at 676 nm, which obviously increases and narrows, finally resulting in a small full width at half maximum (FWHM) of 6.5 nm. This emission wavelength agrees with the SE signal in the fs-TA spectrum, and moreover, the dependence of FWHM *versus* pump energy and the nonlinear gain of emission peak intensity *versus* pump energy are obtained. These results undoubtedly verify the ASE activity of **1**, and the threshold is determined to be 120 kW cm^{-2}. This threshold value is relatively high, but comparable to that of several large-size PAHs and our reported boron-doped molecular carbon (Table S5†).[24–29,61,62] Furthermore, almost no changes are observed for the ASE intensities of this **1**/PS blend

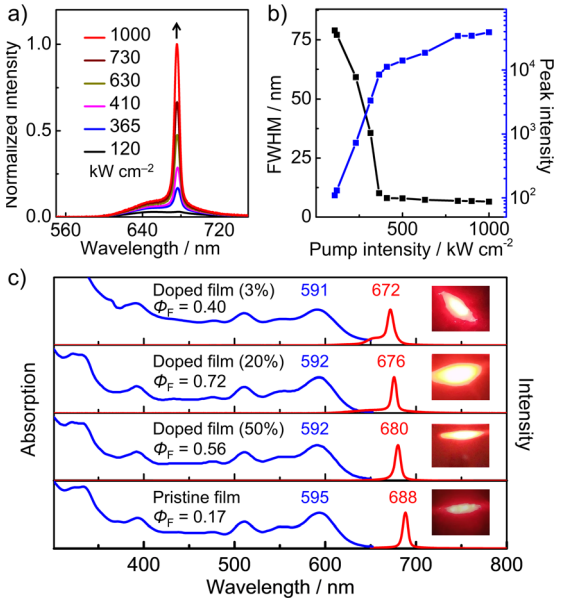

Fig. 6 (a) Photoluminescence spectra of the **1**/PS blend film (20 wt%) taken at different laser energies. (b) Dependences of FWHM and emission peak intensity on the laser energies of the **1**/PS blend film (20 wt%). (c) Absorption spectra (blue) and ASE spectra (red) for the blend and pure films of **1**.

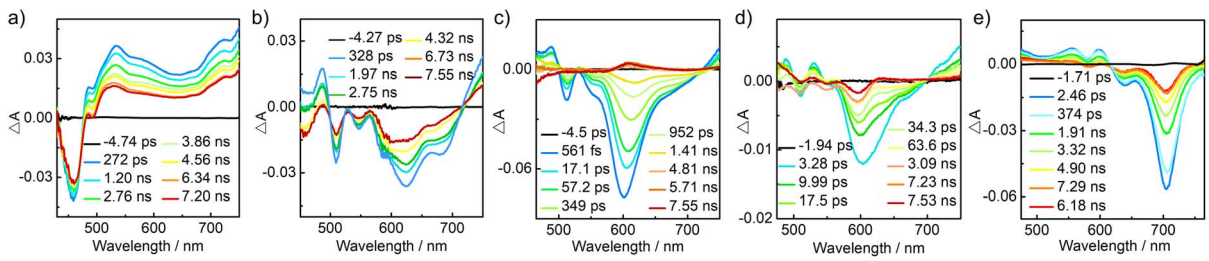

Fig. 5 Femtosecond transient absorption spectra of (a) **6** in toluene, (b) **1** in toluene, (c) the **1**/PS blend film (20 wt%) and (d) the pristine film of **1**, as well as (e) **2** in toluene.

film upon irradiation for 20 min under air at a laser energy of 500 kW cm^{-2} (Fig. S12†), indicative of its remarkable photostability. To our knowledge, it is the first example of ASE-active [*n*]helicene ($n \geq 6$). For **6** and **2**, they do not display any ASE signals, in consistence with their unobserved excited-state SE behaviors.

Finally, to reveal the remarkable effects of double [6]helicene substructures, we studied the photophysical properties of **1** at various film states. The blend films with different doped concentrations and the pure film exhibit very similar absorption spectra with the long-wavelength absorption peak around 590 nm (Fig. 6c), which is also almost identical to that of **1** in toluene. Moreover, the emission peaks of its films and solution all appear at *ca.* 619 nm (Fig. S8†). The fluorescence quantum yields of the 3 wt%, 20 wt% and 50 wt% blend films are 0.40, 0.72 and 0.56, respectively, which are higher than that of the pure film ($\Phi_F = 0.17$) and the solution ($\Phi_F = 0.22$). These results suggest that the molecules are well dispersed and fixed into the PS matrix, leading to the restricted vibration of helicene moieties and the rotation of the tip groups, which can minimize non-radiative decay channels of the excited state. For the pure film, the helicene substructures along with the peripheral substituents effectually inhibit intermolecular π–π stacking and molecular aggregation, further depressing the intermolecular charge-transfer process and preventing fluorescence quenching to a certain extent. We then conducted ASE measurements on the blend and pure films of **1**. These films show the typical dependences of FWHM and emission peak intensity *versus* pump energy. The ASE wavelengths are red-shifted from 672 nm to 688 nm (Fig. S11†), and the fluorescence band around 650 nm is quenched for the 50 wt% blend and pristine films. These fluorescence changes are probably due to the formation of a small portion of excimers at higher concentration.[25,68] The threshold value is estimated to be 258 kW cm^{-2} for the 3 wt% blend and 120 kW cm^{-2} for the 50 wt% blend. The radiative constants (k_r) for the 3 wt%, 20 wt% and 50 wt% blend films were determined to be 6.40×10^7 s^{-1}, 1.70×10^8 s^{-1} and 1.30×10^8 s^{-1} (Fig. S13†), respectively. It is thus concluded that a higher radiative rate may lead to a smaller threshold value. Notably, the ASE properties can be achieved for the blend films with distinct doped concentrations and even pristine films of **1**. Until now, for the reported ASE-active PAHs, the preparation of the blend films with low concentration is highly required to recover SE behavior and realize ASE properties.[18,19,24–29] In this study, B-doped carbohelicene **1** displays ASE properties in the various blend films and even pure film. Such robust ASE performance has never been reported for the family of helicenes and has also been rarely observed in PAHs. This demonstrates that B-doped carbohelicenes are very promising to develop film-insensitive ASE-active materials for organic lasers and photonics.

Conclusions

We succeeded in the synthesis of two boron-doped double [6] carbohelicenes, which were designed by fusion of boron-doped π-systems onto helicenes. They have fully fused $C_{58}B_2$ and $C_{86}B_2$ π-conjugated frameworks containing two [6]helicene subunits, respectively. Thus, they can be regarded as a combination of helicene and boron-containing π-systems, and moreover, the $C_{86}B_2$ molecule represents the largest-size helicene-based B-doped PAH. The helicene substructures and boron atoms endow the polycyclic π-systems with delocalized electronic structures and well-tunable ground-state and excited-state photophysical properties. Notably, the $C_{58}B_2$ molecule displays stimulated emission behavior and amplified spontaneous emission properties in the blend films and even pure film, along with good photostability. Therefore, the results demonstrate the potential of boron-doped carbohelicenes as robust ASE-active materials. This study provides a design strategy for functional helicenes using organoboron chemistry, which can be applied to the construction of more sophisticated photonic materials.

Data availability

The data that support the findings of this study are available in the ESI† of this article.

Author contributions

Y. L., Y. W., and C. D. conceived the idea. Y. L. synthesized the compounds and fully evaluated their properties. Y. L., L. Y., Z. F., and J. Y. performed the theoretical calculations. Y. L., Y. W., and C. D. wrote the manuscript, and all authors discussed and commented on the manuscript. C. D. directed the project.

Conflicts of interest

There are no conflicts to declare.

Acknowledgements

This work was supported by the National Natural Science Foundation of China (no. 52373182 and 22175074) and Jilin Scientific and Technological Development Program (no. 20220101054JC).

Notes and references

1 A. Narita, X.-Y. Wang, X. Feng and K. Müllen, *Chem. Soc. Rev.*, 2015, **44**, 6616–6643.
2 M.-W. Wang, W. Fan, X. Li, Y. Liu, Z. Li, W. Jiang, J. Wu and Z. Wang, *ACS Nano*, 2023, **17**, 20734–20752.
3 M. Grzybowski, B. Sadowski, H. Butenschön and D. T. Gryko, *Angew. Chem., Int. Ed.*, 2020, **59**, 2998–3027.
4 H. Ito, Y. Segawa, K. Murakami and K. Itami, *J. Am. Chem. Soc.*, 2019, **141**, 3–10.
5 M. A. Majewski and M. Stępień, *Angew. Chem., Int. Ed.*, 2019, **58**, 86–116.
6 Y. Segawa, H. Ito and K. Itami, *Nat. Rev. Mater.*, 2016, **1**, 15002.
7 T.-H. Shi and M.-X. Wang, *CCS Chem.*, 2021, **3**, 916–931.
8 S. H. Pun and Q. Miao, *Acc. Chem. Res.*, 2018, **51**, 1630–1642.

9 Y. Tanaka, N. Fukui and H. Shinokubo, *Nat. Commun.*, 2020, **11**, 3873.
10 S. Zank, J. M. Fernández-García, A. J. Stasyuk, A. A. Voityuk, M. Krug, M. Solà, D. M. Guldi and N. Martín, *Angew. Chem., Int. Ed.*, 2022, **61**, e202112834.
11 T. Kirschbaum, F. Rominger and M. Mastalerz, *Angew. Chem., Int. Ed.*, 2020, **59**, 270–274.
12 S. Ma, J. Gu, C. Lin, Z. Luo, Y. Zhu and J. Wang, *J. Am. Chem. Soc.*, 2020, **142**, 16887–16893.
13 X.-J. Zhao, H. Hou, X.-T. Fan, Y. Wang, Y.-M. Liu, C. Tang, S.-H. Liu, P.-P. Ding, J. Cheng, D.-H. Lin, C. Wang, Y. Yang and Y.-Z. Tan, *Nat. Commun.*, 2019, **10**, 3057.
14 W. Jiang and Z. Wang, *J. Am. Chem. Soc.*, 2022, **144**, 14976–14991.
15 N. Ogawa, Y. Yamaoka, H. Takikawa, K.-i. Yamada and K. Takasu, *J. Am. Chem. Soc.*, 2020, **142**, 13322–13327.
16 M. Mahl, M. A. Niyas, K. Shoyama and F. Würthner, *Nat. Chem.*, 2022, **14**, 457–462.
17 I. D. W. Samuel and G. A. Turnbull, *Chem. Rev.*, 2007, **107**, 1272–1295.
18 G. M. Paternò, Goudappagouda, Q. Chen, G. Lanzani, F. Scotognella and A. Narita, *Adv. Opt. Mater.*, 2021, **9**, 2100508.
19 G. M. Paternò, L. Moretti, A. J. Barker, Q. Chen, K. Müllen, A. Narita, G. Cerullo, F. Scotognella and G. Lanzani, *Adv. Funct. Mater.*, 2019, **29**, 1805249.
20 B. Liu, M. Chen, X. Liu, R. Fu, Y. Zhao, Y. Duan and L. Zhang, *J. Am. Chem. Soc.*, 2023, **145**, 28137–28145.
21 W. Zeng and J. Wu, *Chem*, 2021, **7**, 358–386.
22 J. Liu and X. Feng, *Angew. Chem., Int. Ed.*, 2020, **59**, 23386–23401.
23 Z. X. Chen, Y. Li and F. Huang, *Chem*, 2021, **7**, 288–332.
24 G. M. Paternò, Q. Chen, X.-Y. Wang, J. Liu, S. G. Motti, A. Petrozza, X. Feng, G. Lanzani, K. Müllen, A. Narita and F. Scotognella, *Angew. Chem., Int. Ed.*, 2017, **56**, 6753–6757.
25 Y. Zou, V. Bonal, S. Moles Quintero, P. G. Boj, J. M. Villalvilla, J. A. Quintana, G. Li, S. Wu, Q. Jiang, Y. Ni, J. Casado, M. A. Díaz-García and J. Wu, *Angew. Chem., Int. Ed.*, 2020, **59**, 14927–14934.
26 V. Bonal, R. Muñoz-Mármol, F. Gordillo Gámez, M. Morales-Vidal, J. M. Villalvilla, P. G. Boj, J. A. Quintana, Y. Gu, J. Wu, J. Casado and M. A. Díaz-García, *Nat. Commun.*, 2019, **10**, 3327.
27 R. Muñoz-Mármol, F. Gordillo, V. Bonal, J. M. Villalvilla, P. G. Boj, J. A. Quintana, A. M. Ross, G. M. Paternò, F. Scotognella, G. Lanzani, A. Derradji, J. C. Sancho-García, Y. Gu, J. Wu, J. Casado and M. A. Díaz-García, *Adv. Funct. Mater.*, 2021, **31**, 2105073.
28 Y. Gu, V. Vega-Mayoral, S. Garcia-Orrit, D. Schollmeyer, A. Narita, J. Cabanillas-González, Z. Qiu and K. Müllen, *Angew. Chem., Int. Ed.*, 2022, **61**, e202201088.
29 X. Xu, G. Serra, A. Villa, R. Muñoz-Mármol, S. Vasylevskyi, M. Gadea, A. Lucotti, Z. Lin, P. G. Boj, R. Kabe, M. Tommasini, M. Á. Díaz-García, F. Scotognella, G. M. Paternò and A. Narita, *Chem. Sci.*, 2022, **13**, 13040–13045.
30 M. Rickhaus, M. Mayor and M. Juríček, *Chem. Soc. Rev.*, 2016, **45**, 1542–1556.
31 Y. Shen and C.-F. Chen, *Chem. Rev.*, 2012, **112**, 1463–1535.
32 M. Gingras, *Chem. Soc. Rev.*, 2013, **42**, 1051–1095.
33 G.-F. Huo, T. M. Fukunaga, X. Hou, Y. Han, W. Fan, S. Wu, H. Isobe and J. Wu, *Angew. Chem., Int. Ed.*, 2023, **62**, e202218090.
34 T. Fujikawa, Y. Segawa and K. Itami, *J. Am. Chem. Soc.*, 2015, **137**, 7763–7768.
35 S. Jia, S. Li, Y. Liu, W. Qin and H. Yan, *Angew. Chem., Int. Ed.*, 2019, **58**, 18496–18501.
36 T. Hosokawa, Y. Takahashi, T. Matsushima, S. Watanabe, S. Kikkawa, I. Azumaya, A. Tsurusaki and K. Kamikawa, *J. Am. Chem. Soc.*, 2017, **139**, 18512–18521.
37 B. Liu, M. Böckmann, W. Jiang, N. L. Doltsinis and Z. Wang, *J. Am. Chem. Soc.*, 2020, **142**, 7092–7099.
38 W. Yang, N. Li, J. Miao, L. Zhan, S. Gong, Z. Huang and C. Yang, *CCS Chem.*, 2022, **4**, 3463–3471.
39 J. Wang, C. Shen, G. Zhang, F. Gan, Y. Ding and H. Qiu, *Angew. Chem., Int. Ed.*, 2022, **61**, e202115979.
40 M. Navakouski, H. Zhylitskaya, P. J. Chmielewski, T. Lis, J. Cybińska and M. Stępień, *Angew. Chem., Int. Ed.*, 2019, **58**, 4929–4933.
41 W. Fu, V. Pelliccioli, R. Casares-López, J. M. Cuerva, M. Simon, C. Golz and M. Alcarazo, *CCS Chem.*, 2024, DOI: **10.31635/ccschem.024.202404088**.
42 M. Hirai, N. Tanaka, M. Sakai and S. Yamaguchi, *Chem. Rev.*, 2019, **119**, 8291–8331.
43 L. Ji, S. Griesbeck and T. B. Marder, *Chem. Sci.*, 2017, **8**, 846–863.
44 E. von Grotthuss, A. John, T. Kaese and M. Wagner, *Asian J. Org. Chem.*, 2018, **7**, 37–53.
45 A. Escande and M. J. Ingleson, *Chem. Commun.*, 2015, **51**, 6257–6274.
46 J. M. Farrell, C. Mützel, D. Bialas, M. Rudolf, K. Menekse, A.-M. Krause, M. Stolte and F. Würthner, *J. Am. Chem. Soc.*, 2019, **141**, 9096–9104.
47 T. Huang, Z. Ding, H. Liu, P.-A. Chen, L. Zhao, Y. Hu, Y. Yao, K. Yang and Z. Zeng, *Chin. Chem. Lett.*, 2024, **35**, 109117.
48 N. Ando, T. Yamada, H. Narita, N. N. Oehlmann, M. Wagner and S. Yamaguchi, *J. Am. Chem. Soc.*, 2021, **143**, 9944–9951.
49 Z. Fan, W. Sun, Y. Yang, J. Guo, C. Dou and Y. Wang, *Chin. Chem. Lett.*, 2023, **34**, 107729.
50 F. Miyamoto, S. Nakatsuka, K. Yamada, K.-i. Nakayama and T. Hatakeyama, *Org. Lett.*, 2015, **17**, 6158–6161.
51 C. Dou, S. Saito, K. Matsuo, I. Hisaki and S. Yamaguchi, *Angew. Chem., Int. Ed.*, 2012, **51**, 12206–12210.
52 V. M. Hertz, M. Bolte, H.-W. Lerner and M. Wagner, *Angew. Chem., Int. Ed.*, 2015, **54**, 8800–8804.
53 J.-J. Zhang, L. Yang, F. Liu, G. Serra, Y. Fu, A. Lucotti, A. A. Popov, M. Tommasini, J. Ma and X. Feng, *Angew. Chem., Int. Ed.*, 2023, **62**, e202312055.
54 R. J. Kahan, D. L. Crossley, J. Cid, J. E. Radcliffe, A. W. Woodward, V. Fasano, S. Endres, G. F. S. Whitehead and M. J. Ingleson, *Chem. Commun.*, 2018, **54**, 9490–9493.

55 D. L. Crossley, R. J. Kahan, S. Endres, A. J. Warner, R. A. Smith, J. Cid, J. J. Dunsford, J. E. Jones, I. Vitorica-Yrezabal and M. J. Ingleson, *Chem. Sci.*, 2017, **8**, 7969–7977.
56 J. Radtke, K. Schickedanz, M. Bamberg, L. Menduti, D. Schollmeyer, M. Bolte, H.-W. Lerner and M. Wagner, *Chem. Sci.*, 2019, **10**, 9017–9027.
57 M. Schnitzlein, K. Shoyama and F. Würthner, *Chem. Sci.*, 2024, **15**, 2984–2989.
58 L. Yuan, Y. Wang and C. Dou, *Org. Mater.*, 2023, **5**, 191–201.
59 L. Yuan, J. Guo, Y. Yang, K. Ye, C. Dou and Y. Wang, *CCS Chem.*, 2023, **5**, 876–884.
60 W. Sun, J. Guo, Z. Fan, L. Yuan, K. Ye, C. Dou and Y. Wang, *Angew. Chem., Int. Ed.*, 2022, **61**, e202209271.
61 Y. Liu, L. Yuan, J. Guo, W. Sun, Y. Wang and C. Dou, *Angew. Chem., Int. Ed.*, 2023, **62**, e202306911.
62 Z. Fan, Y. Liu, T. Zhang, Y. Wang and C. Dou, *CCS Chem.*, 2024, DOI: **10.31635/ccschem.024.202403953**.
63 J.-J. Zhang, M.-C. Tang, Y. Fu, K.-H. Low, J. Ma, L. Yang, J. J. Weigand, J. Liu, V. W.-W. Yam and X. Feng, *Angew. Chem., Int. Ed.*, 2021, **60**, 2833–2838.
64 M. Randić, *Chem. Rev.*, 2003, **103**, 3449–3605.
65 A. J. C. Kuehne and M. C. Gather, *Chem. Rev.*, 2016, **116**, 12823–12864.
66 C. Adachi and A. S. D. Sandanayaka, *CCS Chem.*, 2020, **2**, 1203–1216.
67 K. Wang and Y. S. Zhao, *Chem*, 2021, **7**, 3221–3231.
68 R. Muñoz-Mármol, N. Zink-Lorre, J. M. Villalvilla, P. G. Boj, J. A. Quintana, C. Vázquez, A. Anderson, M. J. Gordon, A. Sastre-Santos, F. Fernández-Lázaro and M. A. Díaz-García, *J. Phys. Chem. C*, 2018, **122**, 24896–24906.